

Evolution of Dust and Water Ice in Cometary Comae by Radiative Torques

THIEM HOANG,^{1,2} NGO-DUY TUNG,³

¹*Korea Astronomy and Space Science Institute, Daejeon 34055, Republic of Korea*

²*University of Science and Technology, Korea, (UST), 217 Gajeong-ro Yuseong-gu, Daejeon 34113, Republic of Korea*

³*University of Science and Technology of Hanoi, VAST, 18 Hoang Quoc Viet, Hanoi, Vietnam*

ABSTRACT

Comets provide unique information about the physical and chemical properties of the environment in which the Solar system was formed. Understanding how cometary dust and ice evolve under the effect of sunlight is essential for constraining nuclear structure and triggering mechanism of comet activity. In this paper, we first study rotational disruption of dust grains lifted by outgassing from comet nuclei by radiative torques (RATs). We find that composite grains could be rapidly disrupted into small fragments by the Radiative Torque Disruption (RATD) mechanism. We then study rotational desorption of ice grains by RATs and find that icy grains could be desorbed from large heliocentric distances, beyond the sublimation radius of water at $R_{\text{sub}}(\text{H}_2\text{O}) \sim 3 \text{ AU}$. We also calculate the production rate of water vapor versus the heliocentric distance of comets due to rotational desorption. Our results could explain the variation of dust properties and the presence of small grains frequently observed from cometary comae. Finally, we suggest that the activity of distant comets could be triggered by rotational disruption of grains and desorption of water ice grains at large heliocentric distances.

Keywords: comet, dust, water, ice

1. INTRODUCTION

Comets provide essential information about the physical and chemical properties of the environment in which the Solar system was formed. In general, a comet seen in the night sky includes a small nucleus, an extended coma, and long tails (ion and dust). Comet nuclei are made of dust, water ice, and frozen compounds, which are implied from the "dirty snowball" model (Whipple 1950) or "icy dirtball" model (Keller 1989). Understanding how comet activity is triggered is a longstanding problem in cometary science (see Levasseur-Regourd et al. 2018 and Keller & Kührt 2020 for recent reviews).

The current paradigm for the activity of comets is based on thermal sublimation of frozen compounds present in the comet nucleus. For most of their orbits, comets are far away from the Sun and stay inactive. When they come closer, highly volatile ices such as CO, CO₂, CH₄, NH₃, first evaporate due to solar heating. Outflowing gas thus drags dust and water ice grains off the nucleus, triggering the activity of comets. Such dust and ice grains scatter sunlight, producing an extended glowing region known as the cometary coma.

The properties of dust (size, shape, and composition) and ice in the coma are crucially important for understanding and interpreting observational data. Under-

standing the mechanism of ice-to-gas phase transition is a key to understand the activity triggering of cometary coma. Dust grains in comet nuclei are widely thought of as a conglomerate of small monomers. In the coma, dust properties are expected to be unchanged, whereas water ice grains are expected to be long-lived at large heliocentric distances beyond the sublimation zone of heliocentric distance of $R_{\text{sub}}(\text{H}_2\text{O}) \sim 3 \text{ AU}$ (Hayashi 1981; Yamamoto 1985) due to low temperatures (see Whipple & Huebner 1976; A'Hearn 2011; Mumma & Charnley 2011 for reviews).

Optical-near infrared (NIR) polarimetric observations of scattered sunlight are useful to constrain dust properties from cometary comae. Various observations suggest that the size distribution of comet dust varies over time (see Fulle 2004 and Kronk 2004). Optical observations of Comet 9P/Tempel by Furusho et al. (2007) reveal an increase in the polarization off the center, and they explain it by means of small grains (submicron-sized grains). Gicquel et al. (2012) also found evidence of fragmentation of large grains into smaller ones for this comet. The authors found that small grains of $m < 10^{-14} \text{ g}$ ($a < 0.15 \mu\text{m}$) are much more abundant than predicted by theoretical models. Observations from comet Hale-Bopp by Jones & Gehrz (2000)

suggest grains either compact of size $a < 0.5 \mu\text{m}$ or aggregates of $a < 0.5 \mu\text{m}$. Optical-NIR polarimetric observations by Jones et al. (2008) also reveal the presence of small grains in the cometary coma of COMET 73P/SCHWASSMANN-WACHMANN 3. Furthermore, small grains are detected in this comet through the $10 \mu\text{m}$ silicate emission feature (Mason et al. 2001). The question of how large grains lifted off cometary nuclei could be transformed into smaller ones in the coma as required by observations remains unclear.

In this paper, we will study the evolution of dust grains from cometary comae using the new effect of Radiative Torque Disruption (RATD) discovered by Hoang et al. (2019) (see also Hoang 2019). The RATD mechanism is based on the fact that dust grains of irregular shapes exposed to anisotropic radiation field experience Radiative Torques (RATs; Dolginov & Mitrofanov 1976; Draine & Weingartner 1996; Lazarian & Hoang 2007; Hoang & Lazarian 2008). RATs can spin up the grain to suprathermal rotation (Draine & Weingartner 1996; Abbas et al. 2004) such that the resulting centrifugal stress can exceed the maximum tensile strength of the grain material, which breaks the grain into small fragments (Hoang et al. 2019). Due to its proximity to the radiation source and abundant data from in-situ measurements by spacecraft and remote observations, cometary comae provide a unique test for the RATD mechanism. Very recently, Herranen (2020) studied rotational disruption of fluffy dust grains in comets using radiative torques obtained from numerical calculations and found that rotational disruption is efficient. However, the author did not study the disruption of dust across the coma and disregarded ice grains.

Water ice is an important component of cometary nuclei, which is first proposed seven decades ago by "dirty snowball model" by Whipple (1950) where the nucleus is proposed as a conglomerate of dust and ices. However, recently, a "icy dirtballs" model is introduced based on observations (see Keller & Kührt 2020 for a review). The possible detection of icy grains in cometary nuclei is studied in Hanner (1981) based on thermal sublimation. The author found that the detection of icy grains is possible at distance $R > R_{\text{sub}}(\text{H}_2\text{O})$ from the Sun, where icy grains are not yet heated to sublimation threshold. The existence of icy grains in comets is now established through direct detection by instruments onboard spacecraft (Deep Impact, Schulz et al. 2006; EPOXI, A'Hearn et al. 2011; Rosetta, Schulz et al. 2015) or spectroscopic observation of water ice absorption feature (e.g., Yang et al. 2009).

Understanding how and where water ice is transformed into water vapor is essential for accurate deter-

mination of water ice content. The current paradigm is that the activity of comets is triggered by thermal sublimation of water ice. However, as shown in Hoang & Tram (2020) and Hoang & Tung (2019), ice mantles could be desorbed by rotational desorption at lower temperatures than classical sublimation. Thus, the rotational desorption would dramatically affect the water production rate and accurate determination of water content in comet nuclei from observations. Rotational desorption could be a new mechanism to trigger the activity of comets.

The structure of the paper is as follows. In Section 2, we show the comet model adopted in our paper. In Section 3, we review the disruption mechanism of dust grains and present results. Section 4 is devoted to studying desorption of ice mantles from grains. An extended discussion of our results is presented in Section 5. A summary of our main results is presented in Section 6.

2. PHYSICAL MODEL OF A COMETARY COMA

The cometary coma is assumed to be spherical in which gas and dust are being produced continuously from the nucleus due to heating by solar radiation. Highly volatile ice, such as CO and CO_2 , is expected to evaporate first and lift dust and water ice grains off the nucleus. Since the nucleus presumes to be heated symmetrically by sunlight because its rotation period ($\sim 10^4$ s) is much shorter than the orbital period ($\sim 10^6$ s), gas and dust are expanding symmetrically in the radial direction.

Let Q_{gas} be the rate of mass production by the cometary nucleus and v_{gas} be the expansion velocity of gas. The gas mass density at distance r from the nucleus (i.e., cometocentric distance) can be described by the Haser model (Haser 1957; see also Cochran 1985):

$$\rho_{\text{gas}} = \frac{Q_{\text{gas}}}{4\pi v_{\text{gas}} r^2} \exp\left(-\frac{r}{L_g}\right), \quad (1)$$

where $dM = \rho_{\text{gas}} 4\pi r^2 v_{\text{gas}} dt = Q_{\text{gas}} dt$ is the mass produced during the time interval dt , L_g is the ionization length scale, which is between $1 - 2 \times 10^6$ km (see Laakso 1991). Above, the exponential term describes the decay of gas, and the subdominant effect of solar radiative pressure on the expanding gas is disregarded. For a coma with the radius $r \ll L_g$, we can ignore the exponential term in Equation (1). Physical parameters for a coma are listed in Table 1.

The gas production rate increases with decreasing distance R from the Sun (hereafter heliocentric distance) due to the dependence of radiation flux as $1/R^2$. In general, Q_{gas} increases with decreasing the heliocentric

Table 1. Model parameters for a cometary coma

Parameters	Values
Radius of nucleus, r_n	1 km
Star temperature	$T_{\text{eff}} = 5800 \text{ K}$
Star luminosity	$L = L_{\odot}$
Star radius	$R = R_{\odot}$
Gas density	$n = n_0 (r_n/r)^2$ ^a
Gas temperature	$T_{\text{gas}} = 300 \text{ K}$
Expansion velocity	$v_{\text{gas}} = 0.58(R/1 \text{ AU})^{-0.5} \text{ km s}^{-1}$

^a Here $n_0 = 4 \times 10^{12} \text{ cm}^{-3}$ at $r_n = 1 \text{ km}$ for $Q_{\text{gas}} = 9 \times 10^4 \text{ g s}^{-1}$.

distance R due to solar radiation as

$$Q_{\text{gas}} = Q_0 \left(\frac{R}{1 \text{ AU}} \right)^{-\alpha}, \quad (2)$$

where Q_0 is the gas mass rate at 1 AU, and $\alpha \sim 2 - 4$ (see [Sanzovo et al. 2001](#)). We assume a set of values of $Q_0 = 2.5 \times 10^5 \text{ g cm}^{-3}$ and $\alpha = 3.7$ for the 1961 apparition of the Comet 2P/Encke ([Sanzovo et al. 2001](#)).

The decrease of the radiation flux with increasing heliocentric distance also results in the variation of the gas expansion velocity with R , which can be estimated by a power law ([Delsemme 1982](#)) as

$$v_{\text{gas}} \simeq 0.58 \left(\frac{R}{1 \text{ AU}} \right)^{-0.5} \text{ km s}^{-1}, \quad (3)$$

and the variation of v_{gas} with the cometodistance is ignored for simplicity.

The number density of nucleon in the cometary coma is then given by

$$n_{\text{H}} = \frac{\rho_{\text{gas}}}{\mu m_{\text{H}}} = n_0 \left(\frac{r}{r_n} \right)^{-2} \exp \left(-\frac{r}{L_g} \right), \quad (4)$$

where n_0 is the density at nucleus radius r_n , μ is the mean molecular weight with $\mu = 1$ for purely hydrogen gas and $\mu = 1.4$ for gas of 10% He, and $\mu = 28$ for purely CO gas.

Since the mean free path of gas molecules in the inner coma ($n \sim 10^{10} - 10^{12} \text{ cm}^{-3}$) is much smaller than the grain size (high density), dust in the nucleus is accelerated by molecular drag force and dragged away by the gas flow. Dust is decoupled from the gas at some distance from the nucleus and achieves terminal velocity at a distance of tens of the nucleus radius, which is between 20 and 100 km (see e.g., [Finson & Probstein 1968](#)).

3. ROTATIONAL DISRUPTION OF COMETARY DUST

We first study disruption of aggregate dust grains due to radiative torques.

3.1. Rotational disruption mechanism

The basic idea of the rotational disruption mechanism is as follows. A spherical dust grain of mass density ρ rotating at angular velocity ω develops a centrifugal stress due to centrifugal force, which scales as $S = \rho a^2 \omega^2 / 4$ ([Hoang et al. 2019](#)). When the rotation rate increases to a critical limit such that the tensile stress induced by centrifugal force exceeds the maximum tensile stress, the so-called tensile strength of the material, the grain is disrupted instantaneously. The critical angular velocity for the disruption is given by

$$\begin{aligned} \omega_{\text{cri}} &= \frac{2}{a} \left(\frac{S_{\text{max}}}{\rho} \right)^{1/2} \\ &\simeq 10^9 a_{-6}^{-1} \hat{\rho}^{-1/2} S_{\text{max},9}^{1/2} \text{ rad/s}, \end{aligned} \quad (5)$$

where S_{max} is the tensile strength of dust material and $S_{\text{max},9} = S_{\text{max}} / (10^9 \text{ erg cm}^{-3})$ is the tensile strength in units of $10^{10} \text{ erg cm}^{-3}$. The exact value of S_{max} depends on the dust grain composition and structure. Compact grains can have higher S_{max} than porous/composite grains. Ideal material without impurity, such as diamond, can have $S_{\text{max}} \geq 10^{11} \text{ erg cm}^{-3}$ (see [Hoang et al. 2019](#) for more details).

3.2. Rotation rate of irregular grains spun-up by radiative torques

Grains subject to the anisotropic radiation field experience RATs which act to spin-up the grains to suprathermal rotation ([Dolginov & Mitrofanov 1976](#); [Draine & Weingartner 1996](#); [Lazarian & Hoang 2007](#); [Hoang & Lazarian 2008](#)). To describe the strength of a radiation field, let define $U = u_{\text{rad}} / u_{\text{ISRF}}$ with $u_{\text{ISRF}} = 8.64 \times 10^{-13} \text{ erg cm}^{-3}$ being the energy density of the average interstellar radiation field (ISRF) in the solar neighborhood as given by [Mathis et al. \(1983\)](#). Thus, the typical value for the ISRF is $U = 1$. We consider comets approaching the Sun with $L_{\star} = L_{\odot}$, $R_{\star} = R_{\odot}$, $T_{\star} = 5800 \text{ K}$, $M_{\star} = M_{\odot}$.

Let u_{λ} be the spectral energy density of radiation field at wavelength λ . The radiation energy density at heliocentric distance R is given by

$$u_{\text{rad}} = \frac{L_{\star}}{4\pi R^2 c} \simeq 4.5 \times 10^{-7} \left(\frac{L_{\star}}{L_{\odot}} \right) \left(\frac{R}{1 \text{ AU}} \right)^{-2} \text{ erg cm}^{-3} \quad (6)$$

which corresponds to

$$U = 5.2 \times 10^7 \left(\frac{R}{1 \text{ AU}} \right)^{-2}. \quad (7)$$

The mean wavelength of the radiation field is

$$\bar{\lambda} = \frac{\int u_{\lambda} \lambda d\lambda}{\int u_{\lambda} d\lambda} \quad (8)$$

which yields $\bar{\lambda} \sim 0.91 \mu\text{m}$ for the solar-type star.

In the plasma, grain rotation experiences damping due to collisions with gas species. The well-known damping process for a rotating grain is sticking collisions with gas atoms, followed by thermal evaporation. Thus, for a gas with He of 10% abundance, the characteristic damping time is

$$\begin{aligned} \tau_{\text{gas}} &= \frac{3}{4\sqrt{\pi}} \frac{I}{1.2n_{\text{H}}m_{\text{H}}v_{\text{th}}a^4} \\ &\simeq 2200 \left(\frac{\hat{\rho}a_{-5}}{n_{\text{8}}T_2^{1/2}} \right) \text{ days,} \end{aligned} \quad (9)$$

where $\hat{\rho} = \rho/(3\text{g cm}^{-3})$ with ρ being the dust mass density, $v_{\text{th}} = (2k_{\text{B}}T_{\text{gas}}/m_{\text{H}})^{1/2}$ is the thermal velocity of a gas atom of mass m_{H} in a plasma with temperature T_{gas} and nucleon density n_{H} , the spherical grains are assumed (Hoang & Lazarian 2009; Draine & Weingartner 1996). Above, $a_{-5} = a/(10^{-5}\text{cm})$, $n_{\text{8}} = n_{\text{H}}/(10^8\text{cm}^{-3})$, $T_2 = T_{\text{gas}}/100\text{K}$.

This time is equal to the time required for the grain to collide with an amount of gas of the grain mass.

IR photons emitted by the grain carry away part of the grain's angular momentum, resulting in the damping of the grain rotation. For strong radiation fields or not very small sizes, grains can achieve equilibrium temperature, such that the IR damping coefficient (see Draine & Lazarian 1998) can be calculated as

$$F_{\text{IR}} \simeq 5.5 \times 10^{-3} \left(\frac{U_7^{2/3}}{n_{\text{8}}T_2^{1/2}} \right) a_{-5}, \quad (10)$$

which implies subdominance of the IR damping over the gas damping for $n_{\text{H}} > 10^6\text{cm}^{-3}$ and $U < 10^7$.

Other rotational damping processes include plasma drag, ion collisions, and electric dipole emission. These processes are mostly important for PAHs and very small grains (Draine & Lazarian 1998; Hoang et al. 2010; Hoang et al. 2011). Thus, the total rotational damping rate by gas collisions and IR emission can be written as

$$\tau_{\text{damp}}^{-1} = \tau_{\text{gas}}^{-1}(1 + F_{\text{IR}}). \quad (11)$$

For the radiation source with stable luminosity considered in this paper, radiative torques Γ_{RAT} is constant, and the grain velocity is steadily increased over time. The equilibrium rotation can be achieved at (see Lazarian & Hoang 2007; Hoang & Lazarian 2009; Hoang & Lazarian 2014):

$$\omega_{\text{RAT}} = \frac{\Gamma_{\text{RAT}}\tau_{\text{damp}}}{I}, \quad (12)$$

where $I = 8\pi\rho a^5/15$ is the grain inertia moment.

Following Hoang et al. (2019) and Hoang (2019), the rotation rate by RATs for an unidirectional radiation of $\gamma = 1$ is given by

$$\begin{aligned} \omega_{\text{RAT}} &\simeq 3.2 \times 10^8 a_{-5}^{0.7} \bar{\lambda}_{0.5}^{-1.7} \\ &\times \left(\frac{U_7}{n_{\text{8}}T_2^{1/2}} \right) \left(\frac{1}{1 + F_{\text{IR}}} \right) \text{ rad s}^{-1}, \end{aligned} \quad (13)$$

for grains with $a \lesssim a_{\text{trans}}$, and

$$\begin{aligned} \omega_{\text{RAT}} &\simeq 1.6 \times 10^9 \frac{1}{a_{-5}^2} \bar{\lambda}_{0.5} \\ &\times \left(\frac{U_7}{n_{\text{8}}T_2^{1/2}} \right) \left(\frac{1}{1 + F_{\text{IR}}} \right) \text{ rad s}^{-1}, \end{aligned} \quad (14)$$

for grains with $a > a_{\text{trans}}$.

3.3. Grain disruption size

By setting $\omega_{\text{RAT}} = \omega_{\text{disr}}$, one obtains the disruption size for an arbitrary radiation field with $a \leq a_{\text{trans}}$:

$$\begin{aligned} \left(\frac{a_{\text{disr}}}{0.1\mu\text{m}} \right)^{1.7} &\simeq 0.11 \bar{\lambda}_{0.5}^{1.7} S_{\text{max},7}^{1/2} \\ &\times (1 + F_{\text{IR}}) \left(\frac{n_{\text{8}}T_2^{1/2}}{U_7} \right), \end{aligned} \quad (15)$$

which depends on the local gas density, temperature, and the grain tensile strength S_{max} .

Due to the decrease of the rotation rate for $a > a_{\text{trans}}$, there exist a maximum size of grains that can still be disrupted by centrifugal stress (Hoang & Tram 2020):

$$a_{\text{disr,max}} \simeq 5.0\gamma \bar{\lambda}_{0.5} \left(\frac{U_7}{n_{\text{8}}T_2^{1/2}} \right) \left(\frac{1}{1 + F_{\text{IR}}} \right) \hat{\rho}^{1/2} S_{\text{max},7}^{-1/2} \mu\text{m}. \quad (16)$$

Equation (15) implies that grain disruption occurs as long as $n_{\text{H}}T^{1/2} < U$. For comets at $R \sim 1 - 2\text{AU}$, $U \sim 5 \times 10^7$. Therefore, grains in the $n_{\text{H}} < 5 \times 10^7\text{cm}^{-3}$ regions of the coma can be disrupted. Using Equation (1) one can see that the regions of $r > 250\text{km}$ for $a = 0.1\mu\text{m}$. Larger grains of $a \sim 0.5\mu\text{m}$ can be disrupted at smaller radii.

3.4. Disruption time and lifetime of grains

In the absence of rotational damping, the characteristic timescale for rotational desorption can be estimated as:

$$\begin{aligned} t_{\text{disr},0} &= \frac{I\omega_{\text{disr}}}{dJ/dt} = \frac{I\omega_{\text{disr}}}{\Gamma_{\text{RAT}}} \\ &\simeq 2.1(\gamma U_7)^{-1} \bar{\lambda}_{0.5}^{1.7} \hat{\rho}_{\text{ice}}^{1/2} S_{\text{max},7}^{1/2} a_{-5}^{-0.7} \text{ days} \end{aligned} \quad (17)$$

for $a_{\text{disr}} < a \lesssim a_{\text{trans}}$, and

$$t_{\text{disr},0} \simeq 0.14(\gamma U_7)^{-1} \bar{\lambda}_{0.5}^{-1} \hat{\rho}_{\text{ice}}^{1/2} S_{\text{max},7}^{1/2} a_{-5}^2 \text{ days} \quad (18)$$

for $a_{\text{trans}} < a < a_{\text{disr,max}}$.

In the presence of rotational damping, the disruption timescale can be obtained by solving $\omega(t) = \omega_{\text{disr}}$, which yields

$$\begin{aligned} t_{\text{disr}} &= -\tau_{\text{damp}} \ln \left(1 - \frac{\omega_{\text{disr}}}{\omega_{\text{RAT}}} \right) \\ &= -\tau_{\text{damp}} \ln \left(1 - \frac{t_{\text{disr},0}}{\tau_{\text{damp}}} \right), \end{aligned} \quad (19)$$

which is applicable for $a_{\text{disr,max}} > a > a_{\text{disr}}$. Note that $t_{\text{disr}} \rightarrow \infty$ for $a = [a_{\text{disr}}, a_{\text{disr,max}}]$ because it takes $t \gg t_{\text{damp}}$ to reach $\omega = \omega_{\text{RAT}}$. One sees that t_{disr} returns to $t_{\text{disr},0}$ when $t_{\text{disr},0} \ll \tau_{\text{damp}}$ which is achieved in strong radiation fields.

3.5. Numerical Results

For composite grains considered here, we assume the typical radius of monomers $a_p = 0.1 \mu\text{m}$. For large composite grains, the tensile strength S_{max} is varied between $10^5 - 10^{10} \text{ erg cm}^{-3}$. For small grains of $a < a_p$, which are expected to be compact, we fix the tensile strength to $S_{\text{max}} \gtrsim 10^9 \text{ erg cm}^{-3}$.

Figure 1 shows the grain disruption size as a function of the cometocentric distance r for different S_{max} and heliocentric distances, R , assuming a typical constant value of $Q_{\text{gas}} = 9 \times 10^4 \text{ g s}^{-1}$ (Rosenbush et al. 2007). The disruption range is defined by the grain size between a_{disr} and $a_{\text{disr,max}}$. For a given heliocentric distance, rotational disruption takes place in the outer region of the cometary coma where the gas density has considerably decreased. The grain disruption size, a_{disr} , decreases rapidly with r , from $a_{\text{trans}} = 0.51 \mu\text{m}$ to a minimum value $\sim a_{\text{disr}} = a_p = 0.1 \mu\text{m}$ (see solid lines). At large r where the gas density decreases to a small value, even compact grains of large tensile strengths $S_{\text{max}} \gtrsim 10^9 \text{ erg cm}^{-3}$ could be disrupted. The maximum disruption size, $a_{\text{disr,max}}$, increases rapidly with r and reaches the threshold $a_{\text{max}} = \bar{\lambda}/0.1 \sim 10 \mu\text{m}$ (see dashed lines). Thus, grains of sizes between $a_{\text{disr}} - a_{\text{disr,max}}$ will be disrupted under the effect of RATD. Moreover, the disruption zone is more extended for grains having lower tensile strengths. At $R = 2 \text{ AU}$, grains can be disrupted only in the region of $r > 10 \text{ km}$, but at $R = 0.1 \text{ AU}$, grains can be disrupted at $r < 10 \text{ km}$ due to larger solar radiation flux.

Figure 2 shows the disruption time as a function of the cometocentric distance, r , for different tensile strengths, S_{max} , and different heliocentric distances, R , assuming

a constant Q_{gas} . For a given R , the disruption time first rapidly decreases with r and quickly becomes saturated at large r where the IR damping becomes dominant over the gas damping. The disruption time increases with increasing S_{max} . For instance, the disruption time is rather short, of $t_{\text{disr}} \lesssim 10 \text{ days}$ at $R = 1 \text{ AU}$, and decreases to $t < 1 \text{ days}$ at $R = 0.1 \text{ AU}$, assuming $S_{\text{max}} \lesssim 10^8 \text{ erg cm}^{-3}$.

To account for the dependence of Q_{gas} on the heliocentric distance, we calculate the disruption size for Q_{gas} described by Equation (2). The results are shown in Figures 3 and 4. The variations of a_{disr} and $a_{\text{disr,max}}$ with radius r are similar as in the case of constant Q_{gas} (Figure 1). However, their variation with R is radically different due to the steep decrease of Q_{gas} with R . Specifically, at small R , grain disruption starts to occur at a much larger radius of $r \sim 100 \text{ km}$ for $R = 0.1 \text{ AU}$. On the other hand, at large distances of $R = 2 \text{ AU}$, grain disruption occurs at small r , of $r \sim 10 \text{ km}$ (see more details in Figure 5).

Similarly, the time it takes to disrupt grains by RATD is of the same order as in Figure 2 for the same heliocentric distance, but the curves are shifted to higher radius because the high gas density prohibits the rotational disruption to occur near the nuclei.

Figure 5 shows the minimum radius where the rotational disruption occurs as a function of the heliocentric distance for the different tensile strength, assuming a constant Q_{gas} (left panel) and varying Q_{gas} (right panel). As expected, weak grains are disrupted even very close to the nuclei ($\sim 8 \text{ km}$ at $R = 0.1 \text{ AU}$ for fluffy grains with $S_{\text{max}} = 10^5 \text{ erg cm}^{-3}$), implying that they could be disrupted as soon as being lifted off by out-gassing. Grains of large tensile strengths, $S_{\text{max}} \gtrsim 10^9 \text{ erg cm}^{-3}$, are disrupted in regions of $r > 100 \text{ km}$. Moreover, for the constant Q_{gas} (left panel), the minimum disruption radius increases with R because of the decrease of the radiation flux. For the varying $Q_{\text{gas}} \propto R^{-3.7}$, r_{min} decreases with R because the gas damping rate decreases faster than the spin-up rate by RATs (right panel). Grain disruption still occurs at large heliodistances of $R > 5 \text{ AU}$.

4. ROTATIONAL DESORPTION OF COMETARY ICE

We now study rotational desorption of water ice grains by radiative torques. Such grains are originally present in cometary nuclei and lifted off by outgassing of highly volatile ices such as CO and CO₂.

4.1. Rotational desorption of icy grain mantles

Here we consider a grain model consisting of an amorphous silicate core covered by a double-layer ice mantle

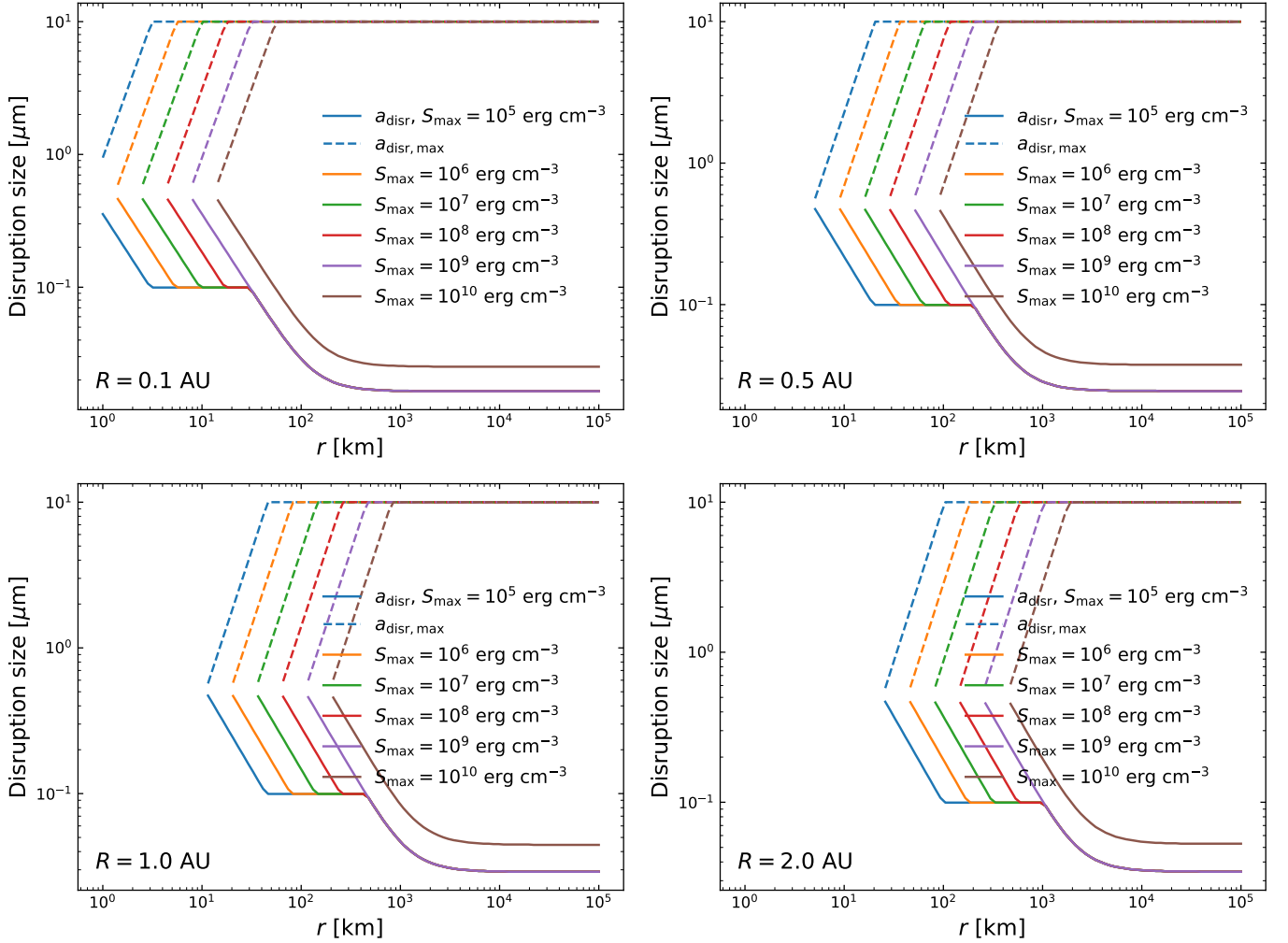


Figure 1. Grain disruption size vs. cometocentric distance for different tensile strengths, S_{\max} , and constant Q_{gas} . The comet is located at different heliocentric distances from $R = 0.1 - 2$ AU. The disruption zone is more extended for weaker grains or smaller R .

(see Figure 6). Let a_c be the radius of silicate core and Δa_m be the average thickness of the mantle. The exact shape of icy grains is unknown, but we can assume that they have irregular shapes as required by strongly polarized H_2O and CO ice absorption features (Chrysotomou et al. 1996; Whittet et al. 2008). Thus, one can define an effective radius of the grain, a , which is defined as the radius of the sphere with the same volume as the grain. The effective grain size is $a \approx a_c + \Delta a_m$. The grain core is assumed to have a typical radius of $0.05 \mu\text{m}$ (Greenberg 1989).

The tensile strength of the bulk ice is $S_{\max} \sim 2 \times 10^7 \text{ erg cm}^{-3}$ at low temperatures. The adhesive strength between the ice mantle and the solid surface has a wide range, depending on the surface properties (Itagaki 1983; Work & Lian 2018).

When the rotation rate is sufficiently high such as the tensile stress exceeds the maximum limit of the ice man-

tle, S_{\max} , the grain is disrupted. The critical rotational velocity is determined by $S_x = S_{\max}$:

$$\omega_{\text{disr}} = \frac{2}{a(1 - x_0^2/a^2)^{1/2}} \left(\frac{S_{\max}}{\rho_{\text{ice}}} \right)^{1/2} \\ \simeq \frac{6.3 \times 10^8}{a_{-5}(1 - x_0^2/a^2)^{1/2}} \hat{\rho}_{\text{ice}}^{-1/2} S_{\max,7}^{1/2} \text{ rad s}^{-1}, \quad (20)$$

where x_0 is the distance from the core-mantle interface to the spinning axis (see Figure 6), $\rho_{\text{ice}} = 1 \text{ g cm}^{-3}$ is the mass density of ice.

Above, we assume that the grain is spinning along the principal axis of maximum inertia moment. This assumption is valid because internal relaxation within the rapidly spinning grain due to Barnett effect rapidly brings the grain axis to be aligned with its angular momentum (Purcell 1979; Roberge & Lazarian 1999).

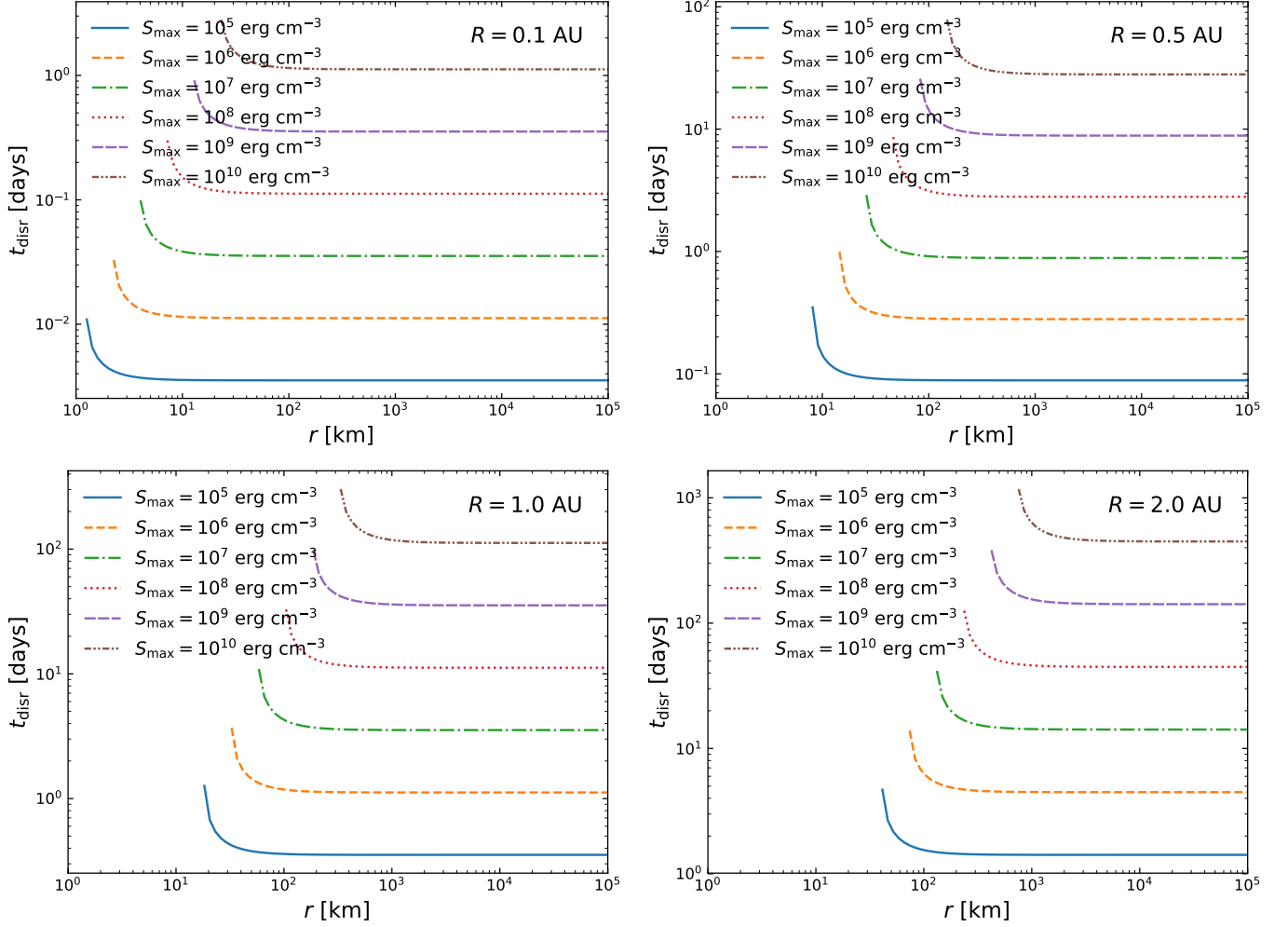


Figure 2. Same as Figure 1, but for the disruption time of $a = 1 \mu\text{m}$ grains. The disruption time decreases with decreasing tensile strength S_{max} and heliocentric distance R .

The grain disruption size of ice mantles is given by

$$a_{\text{disr}} \simeq 0.13 \gamma^{-1/1.7} \bar{\lambda}_{0.5} (S_{\text{max},7} / \hat{\rho}_{\text{ice}})^{1/3.4} (1 + F_{\text{IR}})^{1/1.7} \left(\frac{n_8 T_2^{1/2}}{U_7} \right)^{1/1.7} \mu\text{m}, \quad (21)$$

for $a_{\text{disr}} \lesssim a_{\text{trans}}$ and $x_0 \ll a$, which depends on the local gas density and temperature due to gas damping. The equation indicates that all grains in the size range $a_{\text{trans}} > a > a_{\text{disr}}$ would be disrupted.

4.2. Desorption time and lifetime of water ice grains

In the absence of rotational damping, the characteristic timescale for rotational desorption of ice mantles can be estimated from Equation (17):

$$t_{\text{des}} = \frac{I \omega_{\text{disr}}}{\Gamma_{\text{RAT}}} \simeq 2.2 (\gamma U_7)^{-1} \bar{\lambda}_{0.5}^{1.7} \hat{\rho}_{\text{ice}}^{1/2} S_{\text{max},7}^{1/2} a_{-5}^{-0.7} \text{ days} \quad (22)$$

for $a_{\text{disr}} < a \lesssim a_{\text{trans}}$, and

$$t_{\text{des}} \simeq 0.14 (\gamma U_7)^{-1} \bar{\lambda}_{0.5}^{-1} \hat{\rho}_{\text{ice}}^{1/2} S_{\text{max},7}^{1/2} a_{-5}^2 \text{ days} \quad (23)$$

for $a_{\text{trans}} < a < a_{\text{disr,max}}$.

The lifetime of water ice grains is essentially the grain disruption size t_{des} . Therefore, ice grains can survive in the coma in a time of t_{des} .

In the case of non-rotating grains, the lifetime of ice grains is described by thermal sublimation time. For comparison, we also compute the sublimation time of the ice mantle of thickness Δa_m , as given by

$$t_{\text{sub}}(T_d) = - \frac{\Delta a_m}{da/dt} = \frac{\Delta a_m}{l \nu_0} \exp\left(\frac{E_b}{T_d}\right), \quad (24)$$

where $da/dt = l/\tau_{\text{evap}}$ is the rate of decrease in the mantle thickness due to thermal sublimation, l is the thickness of the ice monolayer, and τ_{evap} is the characteristic time that molecules stay on the grain surface before evaporation:

$$\tau_{\text{evap}}^{-1} = \nu_0 \exp\left(\frac{-E_b}{T_d}\right), \quad (25)$$

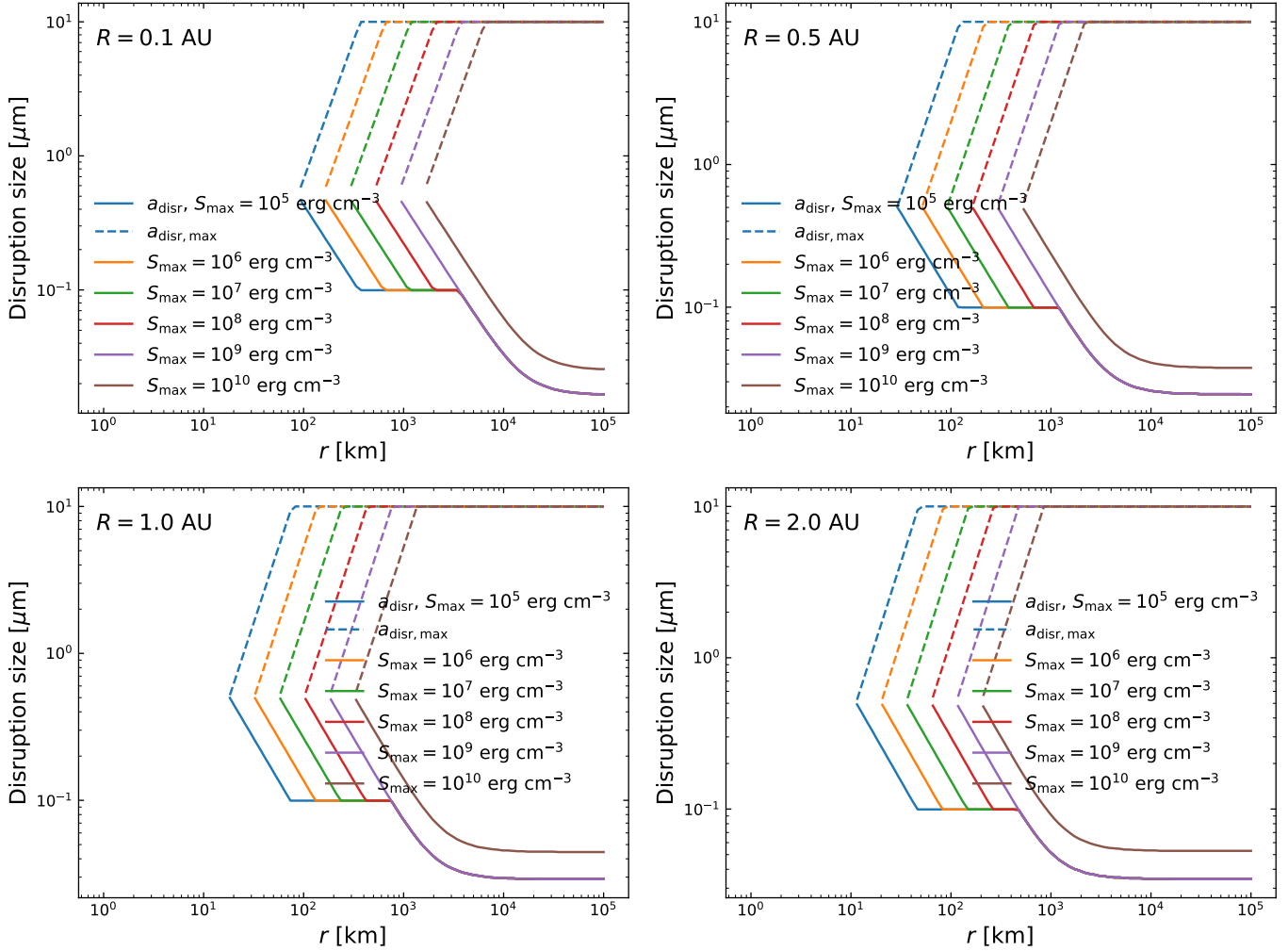


Figure 3. Grain disruption size vs. cometocentric distance, r , for different tensile strengths, assuming varying Q_{gas} . Disruption zone is more extended for larger R due to lower Q_{gas} .

where ν_0 is the characteristic vibration frequency of the lattice, and E_b is the binding energy (Watson & Salpeter 1972).

Plugging the numerical parameters of water ice into the above equation, we obtain

$$t_{\text{sub}} \sim 1.5 \times 10^3 \left(\frac{\Delta a_m}{500 \text{ \AA}} \right) \exp \left(\frac{E_b}{4800 \text{ K}} \frac{100 \text{ K}}{T_d} \right) \text{ yr} \quad (26)$$

For $T_d < 100 \text{ K}$, i.e., $U \sim (T_d/16.4 \text{ K})^6 \lesssim 5 \times 10^4$, Equation (23) yields the desorption time $t_{\text{des}} \sim 27$ days, much shorter than $t_{\text{sub}} > 1500$ yr given by Equation (26).

4.3. Numerical Results

Here, we adopt a conservative value of $S_{\text{max}} = 10^7 \text{ erg cm}^{-3}$ for ice mantles for our numerical calculations. For the grain core, a higher value of $S_{\text{max}} = 10^9 \text{ erg cm}^{-3}$ is adopted.

Figure 7 shows the desorption size of mantles from the grain core, assuming $a_c = 0.05 \mu\text{m}$. Rotational desorption occurs at large distance of $R \sim 5 \text{ AU}$. The inner radius of rotational desorption decreases with Q_{gas} and could reach $r_{\text{des, min}} \sim 1 \text{ km}$ for $Q_{\text{gas}} \sim 10 \text{ g cm}^{-3}$. The small Q_{gas} corresponds to low gas density $n_{\text{gas}}(r)$, which efficiently damps grain rotation spun-up by RATs. For the constant Q_{gas} , the desorption occur at larger radii for larger heliocentric distance R . For the case of varying Q_{gas} , rotational desorption occurs at smaller radii for larger R because the gas production rates decreases more rapidly with R than the decrease of n_{H} with r .

Figure 8 shows the minimum cometocentric distance for which rotational desorption begins to occur r_{min} as a function of the heliodistance for different values of Q_{gas} . At a large distance from the Sun, rotational desorption of ice mantles takes place at a greater cometocentric distance due to the lower radiation flux. For a larger Q_{gas} , the gas density within the coma is higher, thus it

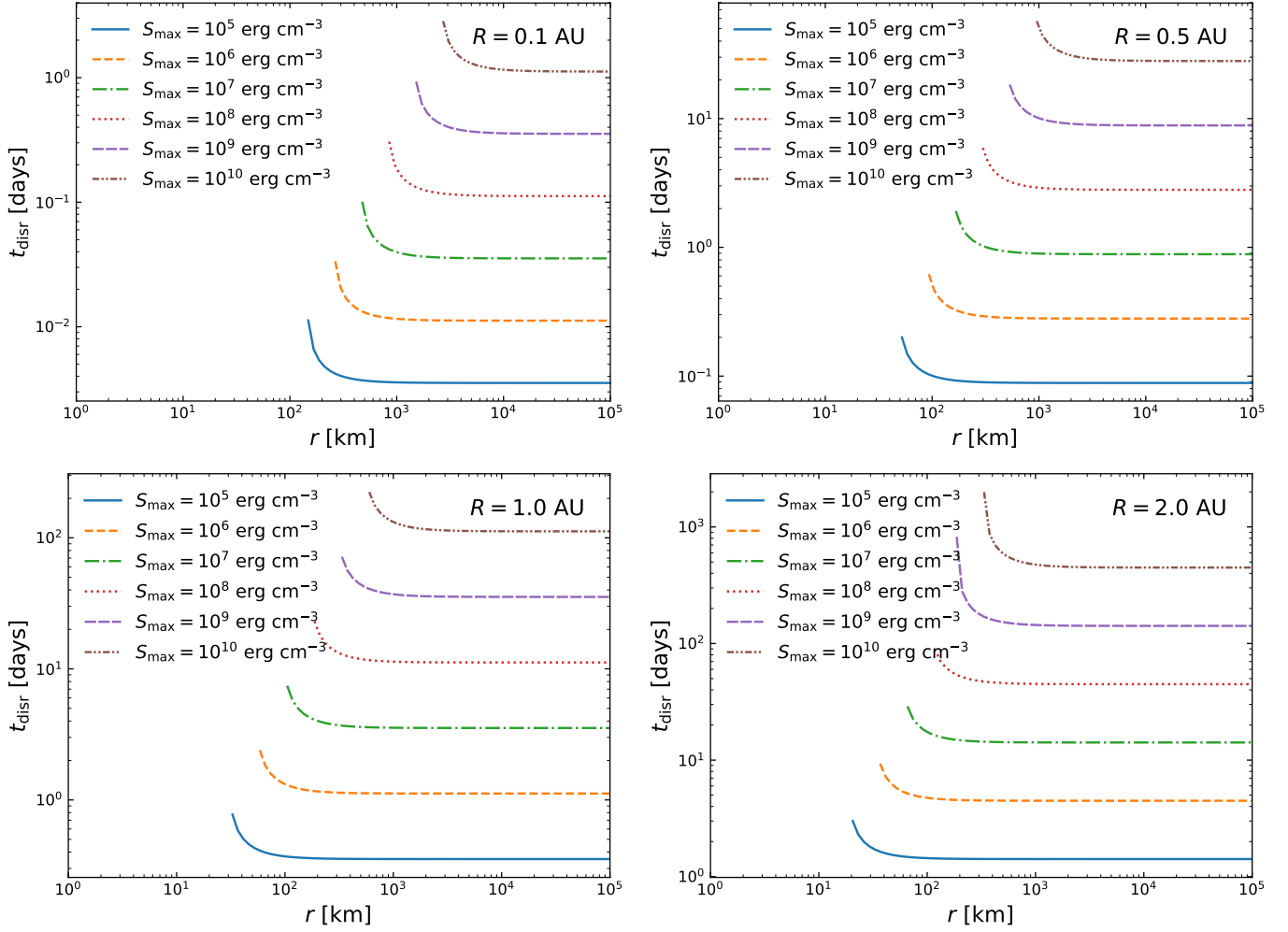


Figure 4. Same as Figure 2 but for varying Q_{gas} . Disruption takes place within the same timescale but at larger radii r for small heliodistances ($R = 0.1, 0.5$ AU) and at smaller radii r for large R (1, 2 AU).

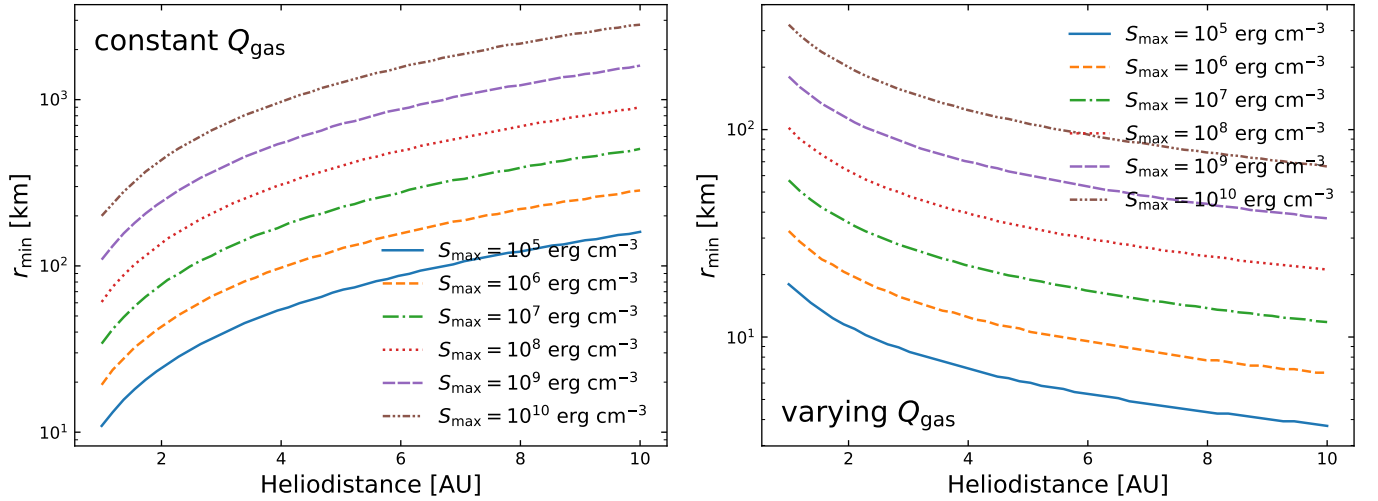


Figure 5. Minimum radius where rotational disruption occurs, r_{min} , as a function of the heliodistance R for two cases of constant Q_{gas} (left panel) and varying Q_{gas} (right panel). r_{min} increases with increasing R and S_{max} .

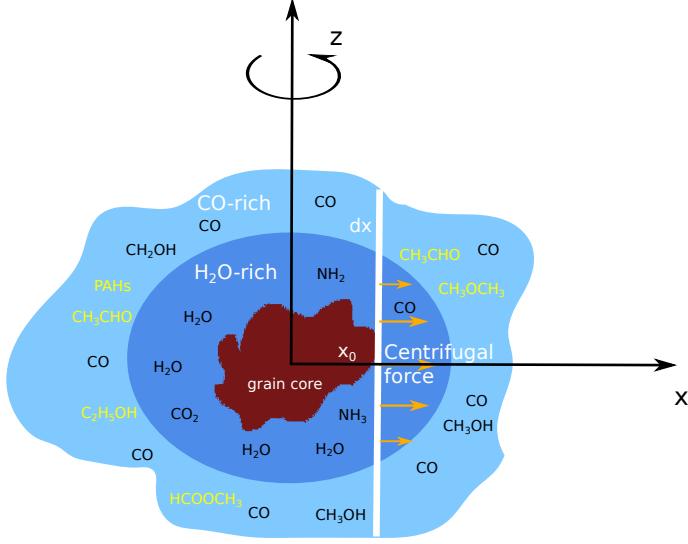


Figure 6. Schematic illustration of a rapidly spinning core-mantle grain of irregular shape, comprising an icy water-rich (blue) and CO-rich (orange) mantle layers. The core is assumed to be compact silicate material, and complex organic molecules are formed in the ice mantle of the core. Centrifugal force field on a slab dx is illustrated, which acts to pull off the ice mantle from the grain core at sufficiently fast rotation.

is harder to desorb ice mantles, increasing the value of r_{\min} .

Figure 9 shows the desorption time of ice mantles from the grain core for the different heliocentric distances. The desorption time increases with increasing R due to the decrease of the radiation flux. The desorption time rapidly decreases with r and achieves a saturated value when the IR damping becomes dominant, similar to the case of grain disruption (see Figure 2).

4.4. Production rate of water vapor via rotational desorption

The production rate of dust and water ice grains is at most equal to Q_{gas} because outgassing can at most lift the equal amount of dust mass. Rotational desorption of ice mantles convert water ice into water vapor. The water vapor production rate, $Q_{\text{H}_2\text{O}}$, is then determined by the mass of water ice produced by desorption.

The water ice production rate due to outgassing is given by

$$Q_{\text{ice}} = \frac{4\pi r^2 dr M_{\text{ice}}(r)}{dt} = 4\pi r^2 v M_{\text{ice}}(r), \quad (27)$$

where the mass of ice grains

$$M_{\text{ice}}(r) \approx \int_{a_{\min}}^{a_{\max}} \left(\frac{4\pi a^3 \rho_{\text{ice}}}{3} \right) \frac{dn_{\text{ice}}}{da} da, \quad (28)$$

where the size distribution of ice grains $dn_{\text{ice}}/da = Ca^{-3.5}$ with C the normalization constant, $a_{\min} = 0.01 \mu\text{m}$ and a_{\max} is varied from $10 \mu\text{m}$. Here the contribution of the grain core to the total mass is negligible because $a_c \ll a_{\max}$.

Then, we calculate the mass of water ice desorbed or water vapor produced as follows:

$$\Delta M_{\text{H}_2\text{O}}(r) = f_{\text{high-J}} \int_{a_{\text{disr}}}^{a_{\text{disr,max}}} \left(\frac{4\pi \rho_{\text{ice}} (a^3 - a_c^3)}{3} \right) \left(\frac{dn_{\text{ice}}}{da} \right) da, \quad (29)$$

where $f_{\text{high-J}}$ is the fraction of grains in the size range $[a_{\min}, a_{\max}]$ that are aligned with high-J attractors by RATs (Hoang & Lazarian 2014). The exact value of $f_{\text{high-J}}$ depends on the grain shape and size, and one expects $0 < f_{\text{high-J}} < 1$ for ordinary paramagnetic grains (Herranen 2020) and $f_{\text{high-J}} = 1$ for grains with iron inclusions (Hoang & Lazarian 2016).

The mass fraction of ice grains desorbed by rotational desorption at cometocentric distance r is given by

$$f_{\text{des,coma}}(r) = \frac{\Delta M_{\text{H}_2\text{O}}(r)}{M_{\text{ice}}(r)}. \quad (30)$$

The total fraction of ice mass removed from the entire coma as a function of the heliocentric distance is obtained by integrating over the cometary coma r :

$$f_{\text{des,helio}}(R) = \frac{\int_{r_{\min}}^{r_{\max}} \Delta M_{\text{H}_2\text{O}}(r) 4\pi r^2 dr}{\int_{r_{\min}}^{r_{\max}} M_{\text{ice}}(r) 4\pi r^2 dr}. \quad (31)$$

Figure 10 shows $f_{\text{des,coma}}$ with the coma radius r (left panel) and $f_{\text{des,helio}}$ (right panel), assuming a conservative value of $f_{\text{high-J}} = 0.5$ and the maximum grain size $a_{\max} = 10 \mu\text{m}$. The core radius is again fixed to $a_c = 0.05 \mu\text{m}$. The amount of ice desorbed $\Delta M_{\text{H}_2\text{O}}$ rapidly reaches maximum $\sim M_{\text{ice}}/2$ at large radii due to the disruption of the very thick mantles of large grains ($\sim 45\%$ of the ice mass).

To account for the fact that comet nuclei may contain very large ice grains, we now consider the maximum grain size of $a_{\max} = 100 \mu\text{m}$. Results are shown in Figure 11. Since rotational desorption is expected to drop for $a \gtrsim \bar{\lambda}/0.1 \sim 10 \mu\text{m}$ due to the decrease of RATs which originates from the canceling effect (see Lazarian & Hoang 2007), the desorption fraction $f_{\text{des,coma}}$ is considerably lower, and the total amount of ice removed within the coma is $f_{\text{des,helio}} \sim 13\%$ of the ice mass.

5. DISCUSSION

5.1. Implications for varying dust properties in cometary comae

Dust grains are lifted off the comet nucleus by the outgassing of highly volatile molecules. Such

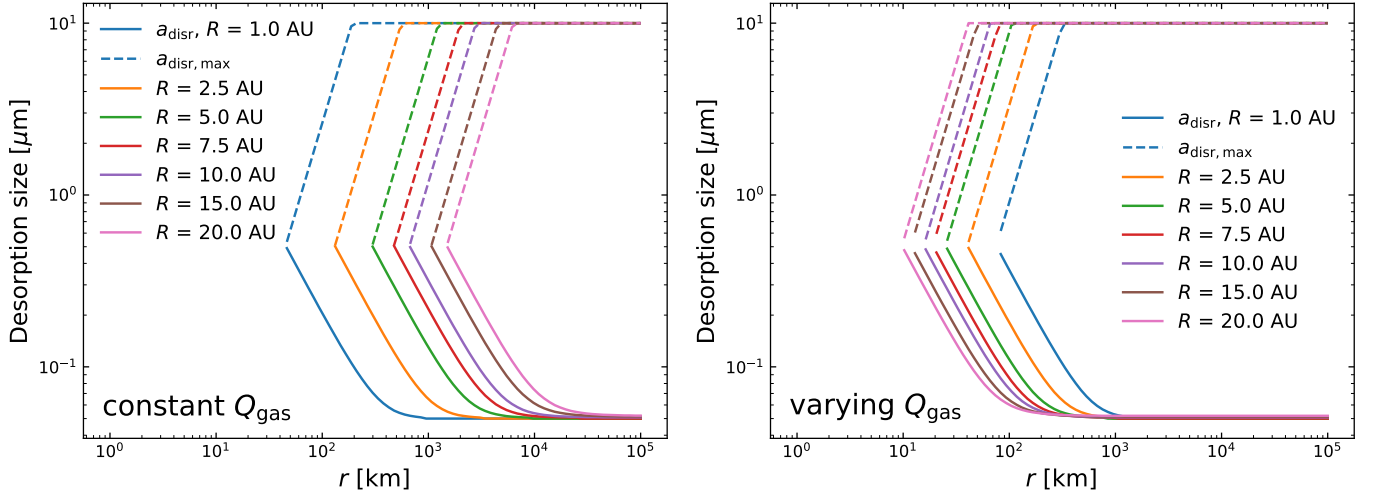


Figure 7. Rotational desorption size of water ice mantles as a function of the cometocentric distance for different heliocentric distances, R , assuming a constant Q_{gas} (left panel) and varying Q_{gas} (right panel). The desorption region is more extended for smaller heliocentric distances in the cases of constant Q_{gas} , but it is reduced when Q_{gas} decreases with increasing R .

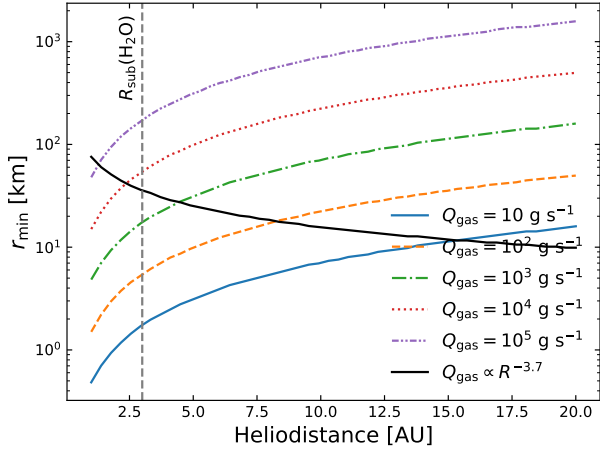


Figure 8. Minimum radius where rotational desorption occurs, r_{min} , as a function of the heliodistance R for different values of Q_{gas} . Black solid line is the plot of r_{min} when the power-law variation of Q_{gas} with R is considered. Rotational desorption could occur well beyond the sublimation zone marked by a vertical line.

grains are presumably thought to have a fluffy structure, made of individual monomers that are loosely bound together via Van der Waals force. Theoretical calculations for the tensile strength of fluffy grains gives $S_{\text{max}} \sim 10^4 (a_p / 0.05 \mu\text{m})^{-2}$ (Hoang 2019) where a_p is the monomer's radius. Experimental measurements in Gundlach et al. (2018) yields $S_{\text{exp}} \simeq 2.73 \times 10^5 (0.1 \mu\text{m} / a_p)$. Thus, one expects a low tensile strength, i.e., $S_{\text{max}} > 10^5 \text{ erg cm}^{-3}$ for larger grains of fluffy structures.

In this paper, using the RATD mechanism, we study the evolution of composite grains assuming different

tensile strengths of $S_{\text{max}} = 10^5 - 10^{10} \text{ erg cm}^{-3}$ for large grains, where the maximum considered values of $S_{\text{max}} \gtrsim 10^9 \text{ erg cm}^{-3}$ are expected for small grains (i.e., $a < 0.1 \mu\text{m}$) of compact structures. We find that RATD is efficient in disrupting large composite grains into smaller ones. Very large grains (VLGs) of fluffy structures of $S_{\text{max}} \lesssim 10^5 \text{ erg cm}^{-3}$ are disrupted as soon as being released from the nucleus by outgassing. Subsequently, smaller grains of higher S_{max} are disrupted at larger r (see Figures 1 and 2). Note that for ordinary paramagnetic or diamagnetic grains, not all large grains are disrupted, but only a fraction of such large grains ($a > a_{\text{disr}}$) that are aligned with high- J attractors, $f_{\text{high-J}}$, could be disrupted. Therefore, the RATD mechanism implies the evolution of dust properties (e.g., grain size distribution and structure), with the decrease (increase) in the abundance of large (small) grains, that depends on the cometocentric and heliocentric distances. Moreover, the efficiency of RATD increases with decreasing the gas production rate Q_{gas} because the latter determines the rotational damping of grains spun-up by RATs.

Observations from spacecraft, as well as polarimetric observations indeed, reveal the variation of dust properties within cometary comae. In-situ measurements by spacecraft report the fragmentation of dust grains on encounter of Comet Haley after released from nucleus (Simpson et al. 1986; Kissel et al. 1986; Tuzzolino et al. 2004). In-situ spacecraft measurements at a distance 8000 km from the nucleus shows the decrease of large grains $m > 10^{-13} \text{ g}$ with distance (Simpson et al. 1986). The COSIMA instrument onboard Rosetta collect dust particles lifted off the nucleus of the Jupiter-family

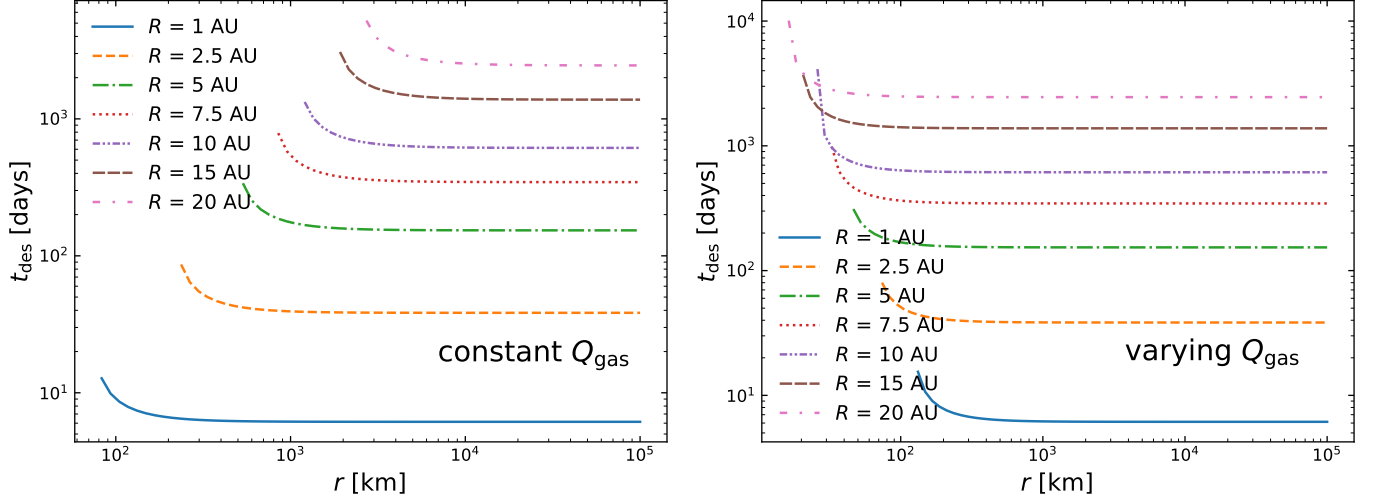


Figure 9. Rotational desorption time of water ice mantles as a function of the cometocentric distance, r , for different heliocentric distances R , assuming a constant Q_{gas} (left panel) and varying Q_{gas} (right panel). Near the Sun, ice grains are desorbed rapidly, while at large R , ice mantles are removed in more than 100 days. Rotational desorption takes place within the same timescale in the two cases, but at different radii due to the different variation of the gas density with R .

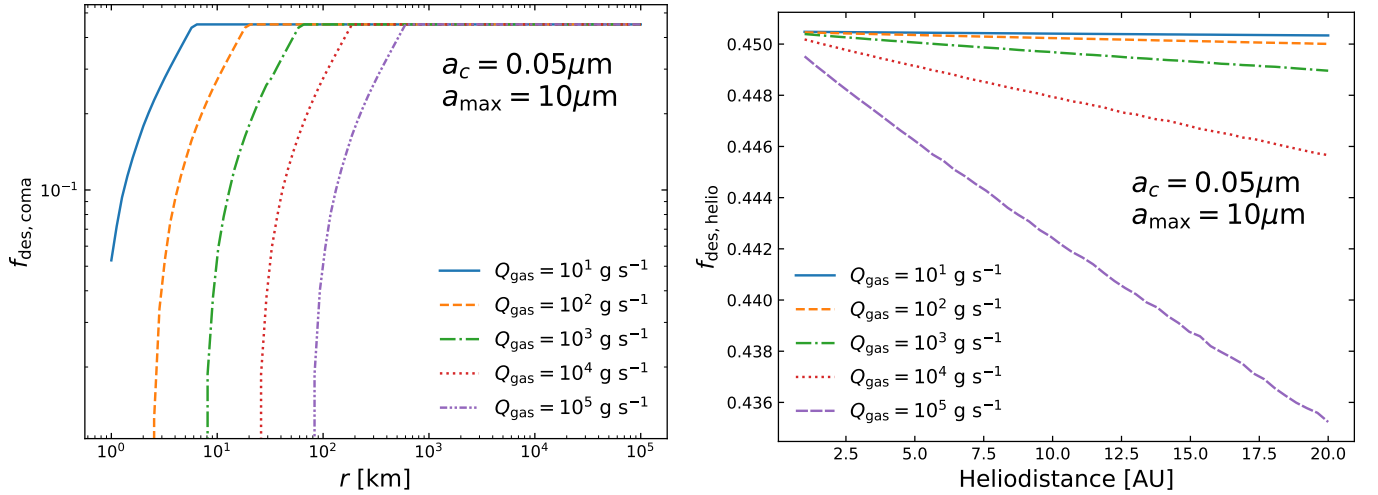


Figure 10. Left panel: Fraction of ice mass removed by rotational desorption, $f_{\text{des,coma}}$, within the coma as a function of the cometocentric distance r . $f_{\text{des,coma}}$ increases rapidly with r and reaches maximum of $\sim f_{\text{high-J}}$. Right panel: Fraction of ice mass removed by rotational desorption $f_{\text{des,helio}}$ as a function of the heliocentric distance R . $f_{\text{des,helio}}$ slightly decreases with increasing R and Q_{gas} . Here $a_{\text{max}} = 10 \mu\text{m}$ is considered.

comet 67P/Churyumov-Gerasimenko, and Schulz et al. (2015) reported that the size of dust grains is a few tens of microns. Therefore, the existence of small grains in the coma must be secondary. Vaisberg et al. (1987) found the spatial and temporal variation of small dust grains in Halley's comet coma with Vega-1 and suggested that those small grains are secondary. Boehnhardt et al. (1990) argued that rotational bursting by radiation pressure proposed by Sekanina & Farrell (1980) is ruled out due to long timescale.

Moreover, polarimetric observations by Jones et al. (2008) reveal the decrease of polarization from the nucleus outward. Jones et al. (2008) performed modeling for comet 73P/SchwassmannWachmann and found that the model with fragmentation can reproduce observed data. Jewitt (2004) also suggested that the disaggregation of porous grains is required to explain the decrease of polarization with the distance. The author also suggested that spin-up by anisotropic gas flow is a mechanism to disrupt grains into smaller ones of $a < 0.1 \mu\text{m}$, although no detailed calculations are pre-

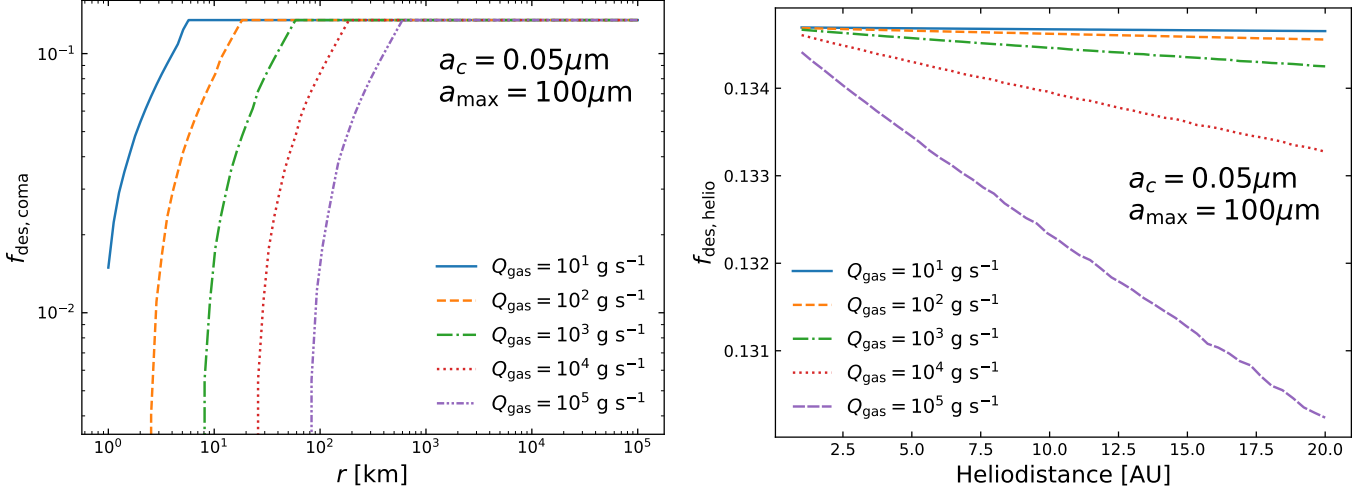


Figure 11. Same as Figure 10 but for $a_{\max} = 100 \mu\text{m}$. The fraction of ice mass removed by rotational desorption is significantly lower since the desorption range $[a_{\text{disr}}, a_{\text{disr,max}}]$ is smaller compared to the grain size distribution range $[0.01 \mu\text{m}, 100 \mu\text{m}]$.

sented. Recently, polarimetric observations by Kwon et al. (2017) and Kwon et al. (2019) reveal the decrease of polarization from the nucleus outward with the cometocentric distance for the inner region of $< 5 \times 10^3 \text{ km}$. The reproduction of small grains from large ones by the RATD mechanism appears to be a plausible mechanism to explain this observational property.

5.2. Implications for desorption water ice from cometary comae

Understanding the desorption mechanism (when and where) of water ice from comets is crucial for accurate determination of the nuclei radius and the volume based on the measurement of water vapor. Future space telescopes with SPHEREx (Doré et al. 2018), LSST, and JWST (United States Congress House Committee on Science & 2011 2018) would provide unprecedented data of water ice and vapor, and an accurate determination of ice requires an accurate understanding of their phase transition. The current model of ice vaporization is based on thermal sublimation from icy grains (Cowan & A’Hearn 1979).

Here, we found that water ice mantles could be desorbed from the grain core by radiative torques. The rotational desorption can occur at heliocentric distances of $R_{\text{des}} \sim 20 \text{ AU}$ (see Figure 8), much larger than the water sublimation radius, $R_{\text{sub}}(\text{H}_2\text{O}) \sim 3 \text{ AU}$. Thus, if ice grains could be lifted off the nucleus, then they would be rotationally desorbed. We also quantified the fraction of ice grains desorbed by RATD and find that ice grains that are aligned at high-J attractors could be completely desorbed (see Figure 10). Measurements of water vapor production rate at $R > R_{\text{sub}}(\text{H}_2\text{O})$ could provide a test for the rotational desorption mechanism

and constrain the value of $f_{\text{high-J}}$, which provide insight into grain geometry and magnetic properties (Hoang & Lazarian 2016; Herranen 2020).

5.3. Implications for Activity of Centaurs and Distant Comets

Centaurs are icy objects outside Jupiter with a perihelion of $R > 5.2 \text{ AU}$ (Jewitt & Kalas 1998). Some active centaurs are reported in Jewitt & Kalas (1998) and Jewitt et al. (2009). Among 23 centaurs observed by (Jewitt 2009, nine with $R = 5.9 - 8.7 \text{ AU}$ are active. Given their far distance from the Sun, their activity is a puzzle because water ice cannot sublimate, whereas CO and CO₂ are too volatile, which can drive activity at a larger distance. The possibility that the activity triggered by a mechanism different from thermal sublimation of water ice is suggested. The authors proposed that the activity is triggered by the conversion of amorphous ice into the crystalline form accompanied by the release of trapped gas.

Observations by Meech et al. (2009) reveal activity of comets at large heliocentric distances of $R = 5.8, 14 \text{ AU}$, beyond the water sublimation zone of $R_{\text{sub}}(\text{H}_2\text{O}) \sim 3 \text{ AU}$ (Hanner 1981; Womack et al. 2017). The annealing of amorphous ice to crystalline ice during which gas is released is referred to explain the activity of the comet.

Our calculations show that for low Q_{gas} , rotational desorption of ice mantles can occur at $R \sim 20 \text{ AU}$ because of inefficient rotational damping. Note that we assume the presence of water ice grains in the coma and do not discuss the lifting mechanism. However, the low Q_{gas} is consistent with the outgassing of highly volatile ices such as CO and CO₂. Thus, the rotational desorption could trigger active comets at large distances.

Therefore, observations of water vapor at large distances could be possible but require high sensitivity because the amount of water is low due to a small amount of Q_{gas} .

Finally, we find that the amount of water ice desorbed as a function of the heliocentric distance depends on the fraction of grains with high- J , $f_{\text{high-}J}$, which depends on the grain shape and magnetic properties (Hoang & Lazarian 2016; Lazarian & Hoang 2019). Thus, one can constrain the ice grain properties with observational measurements of the water production rate.

6. SUMMARY

We study evolution of dust and water ice grains in comets by radiative torques of sunlight. Our main results are summarized as follows:

- We find that RATD can destroy large dust grains of composite structures in cometary comae, resulting in an increase (decrease) in the abundance of small (large) grains with increasing cometocentric distance due to the decrease of the gas density.
- We suggest the rotational disruption of large grains into small fragments can explain the time-variability of dust properties observed toward cometary comae, as well as the presence of small dust grains in cometary comae.

- We study rotational desorption of ice grains and find that water ice grains could be rotationally desorbed rapidly due to centrifugal stress of radiative torques. The rotational desorption could occur at large heliocentric distances much larger than the sublimation radius, $R_{\text{sub}}(\text{H}_2\text{O}) \sim 3 \text{ AU}$. Thus, water vapor could be observed from comae at larger distances, albeit it requires high sensitivity due to a low amount of mass released from comet nuclei at large distances.
- We suggest the activity of distant comets could be triggered by rotational disruption of dust and ice grains, provided that such grains are lifted off the nucleus by outgassing of highly volatile compounds.

ACKNOWLEDGMENTS

This work was supported by the National Research Foundation of Korea (NRF) grants funded by the Korea government (MSIT) through the Basic Science Research Program (2017R1D1A1B03035359) and Mid-career Research Program (2019R1A2C1087045).

REFERENCES

- Abbas, M. M., Craven, P. D., Spann, J. F., et al. 2004, *ApJ*, 614, 781
- A'Hearn, M. F. 2011, *Annual Review of A&A*, 49, 281
- A'Hearn, M. F., Belton, M. J. S., Delamere, W. A., et al. 2011, *Science*, 332, 1396
- Boehnhardt, H., Fechtig, H., & Vanysek, V. 1990, *A&A*, 231, 543
- Chrysostomou, A., Hough, J. H., Whittet, D. C. B., et al. 1996, *ApJL*, 465, L61
- Cochran, A. L. 1985, *AJ*, 90, 2609
- Cowan, J. J., & A'Hearn, M. F. 1979, *Moon and the Planets*, 21, 155
- Delsemme, A. H. 1982, in *Comets*, ed. L. L. Wilkening (Tucson, AZ: Univ. Arizona Press), 85
- Dolginov, A. Z., & Mitrofanov, I. G. 1976, (*Astronomicheskii Zhurnal*, 19, 758)
- Doré, O., Werner, M. W., Ashby, M. L. N., et al. 2018, *arXiv.org*, arXiv:1805.05489
- Draine, B. T., & Lazarian, A. 1998, *ApJ*, 508, 157
- Draine, B. T., & Weingartner, J. C. 1996, *ApJ*, 470, 551
- Finson, M. J., & Probstein, R. F. 1968, *ApJ*, 154, 327
- Fulle, M. 2004, *Comets II*, 565
- Furusho, R., Ikeda, Y., Kinoshita, D., et al. 2007, *Icarus*, 190, 454
- Gicquel, A., Bockelée-Morvan, D., Zakharov, V. V., et al. 2012, *A&A*, 542, A119
- Greenberg, J. 1989, in *Interstellar Dust: Proceedings of the 135th Symposium of the International Astronomical Union*, 345–
- Gundlach, B., Schmidt, K. P., Kreuzig, C., et al. 2018, *MNRAS*, 479, 1273
- Hanner, M. S. 1981, *International Astronomical Union and American Astronomical Society*, 47, 342
- Haser, L. 1957, *Bulletin de la Societe Royale des Sciences de Liege*, 43, 740
- Hayashi, C. 1981, *Progress of Theoretical Physics Supplement*, 70, 35
- Herranen, J. 2020, *ApJ*, 893, 0
- Hoang, T. 2019, *ApJ*, 876, 13
- Hoang, T., Draine, B. T., & Lazarian, A. 2010, *ApJ*, 715, 1462
- Hoang, T., & Lazarian, A. 2008, *MNRAS*, 388, 117
- Hoang, T., & Lazarian, A. 2009, *ApJ*, 695, 1457
- Hoang, T., & Lazarian, A. 2014, *MNRAS*, 438, 680

- Hoang, T., & Lazarian, A. 2016, *ApJ*, 831, 159
- Hoang, T., Lazarian, A., & Draine, B. T. 2011, *ApJ*, 741, 87
- Hoang, T., & Tram, L. N. 2020, *ApJ*, 891, 38
- Hoang, T., Tram, L. N., Lee, H., & Ahn, S.-H. 2019, *Nature Astronomy*, 3, 766
- Hoang, T., & Tung, N. D. 2019, *ApJ*, 885, 125
- Itagaki, K. 1983, in *US Army Cold Regions Research and Engineering Laboratory*, 1983. CRREL-8326.
- Jewitt, D. 2004, *AJ*, 128, 3061
- Jewitt, D. 2009, *AJ*, 137, 4296
- Jewitt, D., & Kalas, P. 1998, *ApJ*, 499, L103
- Jewitt, D., Yang, B., & Haghighipour, N. 2009, *AJ*, 137, 4313
- Jones, T. J., & Gehrz, R. D. 2000, *Icarus*, 143, 338
- Jones, T. J., Stark, D., Woodward, C. E., et al. 2008, *AJ*, 135, 1318
- Keller, H. U. 1989, In *ESA*, 302
- Keller, H. U., & Kühr, E. 2020, *Space Science Reviews*, 216, 14
- Kissel, J., Brownlee, D. E., Buchler, K., et al. 1986, *Nature*, 321, 336
- Kronk, G. W., ed. 2004, *Physical properties of cometary dust from light scattering and thermal emission*, ed. G. W. Kronk, 577–604
- Kwon, Y. G., Ishiguro, M., Kuroda, D., et al. 2017, *AJ*, 154, 173
- Kwon, Y. G., Ishiguro, M., Kwon, J., et al. 2019, *A&A*, 629, A121
- Laakso, H. 1991, *Journal of Geophysical Research*, 96, 7731
- Lazarian, A., & Hoang, T. 2007, *MNRAS*, 378, 910
- Lazarian, A., & Hoang, T. 2019, *ApJ*, 883, 122
- Levasseur-Regourd, A.-C., Agarwal, J., Cottin, H., et al. 2018, *Space Science Reviews*, 214, #64
- Mason, C. G., Gehrz, R. D., Jones, T. J., et al. 2001, *ApJ*, 549, 635
- Mathis, J. S., Mezger, P. G., & Panagia, N. 1983, *A&A*, 128, 212
- Meech, K. J., Pittichová, J., Bar-Nun, A., et al. 2009, *Icarus*, 201, 719
- Mumma, M. J., & Charnley, S. B. 2011, *ARA&A*, 49, 471
- Purcell, E. M. 1979, *ApJ*, 231, 404
- Roberge, W. G., & Lazarian, A. 1999, *MNRAS*, 305, 615
- Rosenbush, V., Kolokolova, L., Lazarian, A., Shakhovskoy, N., & Kiselev, N. 2007, *Icarus*, 186, 317
- Sanzovo, G. C., de Almeida, A. A., Misra, A., et al. 2001, *MNRAS*, 326, 852
- Schulz, R., Owens, A., Rodriguez-Pascual, P. M., et al. 2006, *A&A*, 448, L53
- Schulz, R., Hilchenbach, M., Langevin, Y., et al. 2015, *Nature*, 518, 216
- Sekanina, Z., & Farrell, J. A. 1980, *AJ*, 85, 1538
- Simpson, J. A., Sagdeev, R. Z., Tuzzolino, A. J., et al. 1986, *Nature*, 321, 278
- Tuzzolino, A. J., Economou, T. E., Clark, B. C., et al. 2004, *Science*, 304, 1776
- United States Congress House Committee on Science, S., & 2011, T. 2018, *James Webb Space Telescope*
- Vaisberg, O. L., Smirnov, V., Omel'Chenko, A., Gorn, L., & Iovlev, M. 1987, *A&A*, 187, 753
- Watson, W. D., & Salpeter, E. E. 1972, *ApJ*, 174, 321
- Whipple, F. L. 1950, *ApJ*, 111, 375
- Whipple, F. L., & Huebner, W. F. 1976, *ARA&A*, 14, 143
- Whittet, D. C. B., Hough, J. H., Lazarian, A., & Hoang, T. 2008, *ApJ*, 674, 304
- Womack, M., Sarid, G., & Wierzbos, K. 2017, *Publications of the Astronomical Society of the Pacific*, 129, 031001
- Work, A., & Lian, Y. 2018, *Progress in Aerospace Sciences*, 1
- Yamamoto, T. 1985, *A&A*, 142, 31
- Yang, B., Jewitt, D., & Bus, S. J. 2009, *AJ*, 137, 4538